Accurate extraction of mobility in carbon nanotube network transistors using C-V and I-V measurements

Jinsu Yoon,[1,a)] Dongil Lee,[2,a)] Chaewon Kim,[3] Jieun Lee,[1] Bongsik Choi,[1] Dong Myong Kim,[1] Dae Hwan Kim,[1] Mijung Lee,[3] Yang-Kyu Choi,[2,b)] and Sung-Jin Choi[1,b)]
[1]*School of Electrical Engineering, Kookmin University, Jeongneung-dong, Seongbuk-gu, Seoul 136-702, South Korea*
[2]*Department of Electrical Engineering, KAIST, Daejeon 305-701, South Korea*
[3]*School of Advanced Materials Engineering, Kookmin University, Seoul 136-702, South Korea*

(Received 18 September 2014; accepted 14 November 2014; published online 24 November 2014)

The mobility of single-walled carbon nanotube (SWNT) network thin-film transistors (TFTs) is an essential parameter. Previous extraction methods for mobility encountered problems in extracting accurate intrinsic mobility due to the uncertainty of the SWNT density in the network channel and the existence of contact resistance at the source/drain electrodes. As a result, efficient and accurate extraction of the mobility in SWNT TFTs is challenging using previous methods. We propose a direct method of extracting accurate intrinsic mobility in SWNT TFTs by employing capacitance-voltage and current-voltage measurements. Consequently, we simply obtain accurate intrinsic mobility within the ink-jet printed SWNT TFTs without any complicated calculations. © *2014 AIP Publishing LLC*. [http://dx.doi.org/10.1063/1.4902834]

Single-walled carbon nanotubes (SWNTs) have been extensively explored for a number of electronic applications owing to their excellent electrical, mechanical, and chemical properties.[1–3] The solution process of random networks in semiconductor-enriched SWNTs for thin-film transistors (TFTs), in particular, shows high promise for large-area and/or printed electronics.[4–6] SWNT TFTs exhibit higher mobility than other TFT channel materials, such as amorphous silicon and organic semiconductors.[7–10] Therefore, attention should be directed to accurately extracting an important parameter, such as mobility, which represents the excellent performance of SWNT TFTs. However, using the conventional extraction methods on the mobility in SWNT TFTs present several challenging issues. If the typical parallel plate model is used, the mobility is frequently under-estimated.[11] Importantly, using a cylindrical model, the mobility is strongly dependent on the SWNT density (Λ_0^{-1}), but it is difficult to choose the exact Λ_0^{-1} value, especially for a low-density SWNT network channel.[2,12,13] Therefore, careful determination of Λ_0^{-1} is important, but it generally results in a large variation of extracted mobility. Moreover, previous reports have shown that the mobility is dependent on the channel length due to contact resistance ($R_{contact}$) at the source/drain electrodes, and therefore it should be excluded in extracting the "intrinsic" mobility in SWNT TFTs.[5,8,14–16]

Emphasizing the significance of accurate intrinsic mobility extraction, we propose a direct method for extracting accurate intrinsic mobility of SWNT TFTs. The proposed method utilizes capacitance-voltage (*C-V*) and current-voltage (*I-V*) measurements and requires no assumption regarding the uncertain SWNT density. Furthermore, we confirm that the intrinsic mobility is almost independent of the channel length when the effect of $R_{contact}$ is excluded. *C-V* and *I-V* measurements have been previously used to extract accurate intrinsic mobility in early attempts to characterize silicon transistors, and it is repeated in this paper for SWNT TFTs to establish accurate intrinsic mobility of SWNT TFTs.

The schematic diagram of the fabricated ink-jet printed SWNT TFT is presented in Figure 1(a). The devices were fabricated on 1.5 × 1.5 cm pieces of silicon wafer, which is highly p-doped as a common back-gate, with a thermally grown 55-nm-thick back-gate oxide (SiO_2) layer. The substrate was first functionalized with a poly-L-lysine solution to form an amine-terminated layer,[17,18] which acts as an effective adhesion layer for the SWNTs. The substrate was then rinsed with deionized (DI) water and isopropanol. The active channel material was deposited by immersion in purified 90% semiconductor-enriched SWNT solution (NanoIntegris, Inc.) for 1 min, followed by a thorough rinse with isopropanol and DI water and drying with flowing nitrogen. The source and drain electrodes were inkjet-printed with silver nanoparticle ink, and a 150 °C annealing process was employed. Next, poly-4-vinylphenol (PVP) was printed onto the surface to define the channel widths. A subsequent oxygen plasma-etching step was used to remove unwanted paths to electrically isolate the devices from one another. Finally, the PVP was sequentially removed with acetone, isopropanol, and flowing nitrogen. The channel lengths (L) and widths (W) ranged from 150 to 450 μm and 250 to 490 μm, respectively. Figure 1(b) shows an optical microscopy image of the fabricated SWNT TFT. An atomic force microscopy (AFM) image of the SWNT network channel in a SWNT TFT is also shown in Figure 1(c).

Figure 2(a) illustrates the drain current (I_{DS})-gate voltage (V_{GS}) characteristics of a total of 70 fabricated SWNT TFTs (L = 150–450 μm, W = 250–490 μm) at a drain voltage (V_{DS}) of −0.5 V. We note that the fabricated SWNT TFTs exhibit hysteresis, thus for consistency, we used the forward sweep for all mobility calculations. The mobility of SWNT

[a)]J. Yoon and D. Lee contributed equally to this work.
[b)]Electronic addresses: ykchoi@ee.kaist.ac.kr and sjchoiee@kookmin.ac.kr. Tel.: +82-2-910-5543. Fax: +82-2-910-4449.

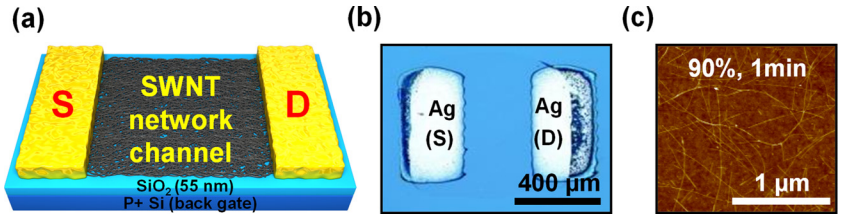

FIG. 1. (a) Device schematic for a back-gate printed SWNT transistor. (b) Optical microscopy image of a SWNT TFT printed on a silicon substrate with a 55-nm-thick gate oxide layer. (c) AFM image ($2.5 \times 2.5\,\mu$m, z-scale is 10 nm) of networks created using the random deposition method with 90% semiconducting nanotube solutions for a deposition time of 1 min.

TFTs can be determined from the I_{DS}–V_{GS} characteristics based upon the previous extraction method using the transconductance ($g_m = \partial I_{DS}/\partial V_{GS}$) with Λ_0^{-1} (Eqs. (1) and (2)), as shown in Figure 2(b). To accurately extract the mobility, meticulous determination of the gate capacitance (C_g) is a prerequisite. The C_g in SWNT TFTs is typically calculated by either the parallel plate model or the more rigorous cylindrical model. For the parallel plate model, which can simply be calculated as ε_{OX}/t_{OX}, where ε_{OX} and t_{OX} are the dielectric constant and thickness, respectively, of the gate insulator, the lack of accuracy is particularly obvious in SWNT TFTs especially with a low density SWNT network. Moreover, the mobility is always underestimated by the parallel plate model compared to the mobility from the cylindrical model, as shown in the red line of Figure 2(b). For a more accurate cylindrical model, calculated considering the electrostatic interaction between SWNTs, a more accurate extracted mobility can be achieved using Eq. (2), where Λ_0^{-1} stands for the density of the SWNTs (4–20 tubes/μm from AFM image), C_Q is the quantum capacitance $(4.0 \times 10^{-10}$ F/m$)^2$, and R is the average diameter of the SWNTs (1.4 nm). However, it seems that the calculated C_g value from a cylindrical model is very sensitive to Λ_0^{-1}, as the black line shows in Figure 2(b).[19] In addition, the density of SWNTs is very difficult to quantify in such a random network, especially with low-density SWNTs. Strictly speaking, the cylindrical model is only expected to be a qualitative guide in SWNT TFTs, but not to hold quantitatively, because the cylindrical model was derived from aligned SWNT devices.[15] Therefore, we performed C-V measurement to extract accurate mobility without the information of Λ_0^{-1}

$$\mu = \frac{L}{V_{DS} C_g W} \frac{\partial I_{DS}}{\partial V_{GS}} = \frac{L}{V_{DS} C_g} \frac{g_m}{W}, \quad (1)$$

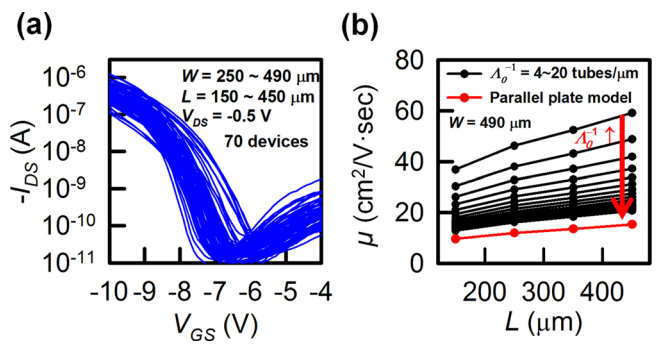

FIG. 2. (a) Transfer characteristic (I_{DS}-V_{GS}) of 70 devices for the deposition condition of 1 min at $V_{DS} = -0.5$ V. (b) The black line is the mobility of a cylindrical model with a variation of Λ_0^{-1} (4–20 tubes/μm), and the red line is the parallel plate model at $L = 150\,\mu$m, 250 μm, 350 μm, and 450 μm; and $W = 490\,\mu$m.

$$C_g = \left\{ C_Q^{-1} + \frac{1}{2\pi\varepsilon_0\varepsilon_{OX}} \ln\left[\frac{\Lambda_0}{R} \frac{\sinh(2\pi t_{OX}/\Lambda_0)}{\pi} \right] \right\}^{-1} \Lambda_0^{-1}. \quad (2)$$

The C-V characteristics of SWNT TFTs with various channel lengths measured at $W = 490\,\mu$m and frequency = 500 Hz are shown in Figure 3(a). Figure 3(b) illustrates the C-V characteristics of the gate to the source/drain (C_G), the gate to the source (C_{GS}), and the gate to the drain (C_{GD}). The minimum values of C_{GS} and C_{GD} are due to the overlap capacitance (C_{OV}) of the gate to the source and the gate to the drain, respectively. Therefore, the minimum value of C_G (C_{min}) in Figures 3(a) and 3(b) is $2 \times C_{OV}$ because it contains both overlaps of C_{GS} and C_{GD}. With the comparison of the measured values, we confirm that the minimum C_G value ($C_{min} = 0.127$ nF) is dominantly caused by the overlap capacitance ($2 \times C_{OV} = 2 \times 0.063$ nF $= 0.126$ nF). Thus, we subtract C_{min} from the measured C_G to consider only the channel capacitance and then integrate the C_G–C_{min} and divide it by W and L to extract the quantity of mobile

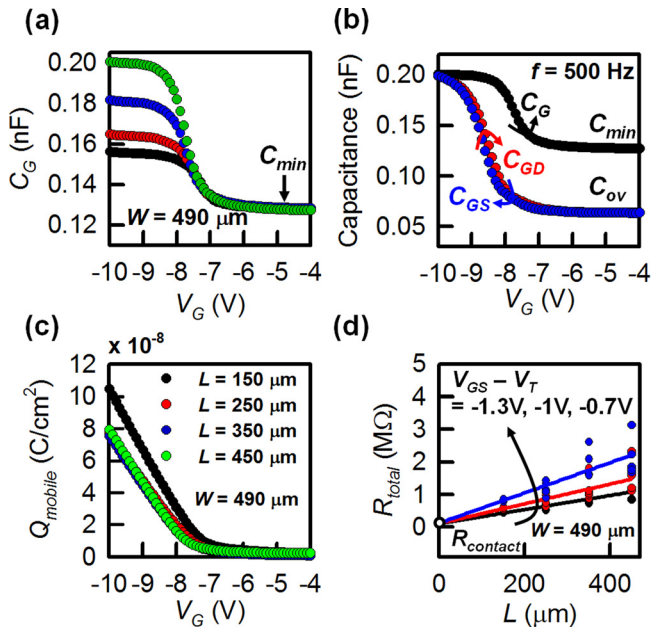

FIG. 3. (a) C-V characteristics of SWNT TFTs with various channel lengths ($L = 150\,\mu$m, 250 μm, 350 μm, 450 μm) measured at 500 Hz. (b) C-V characteristics of SWNT TFTs with $L = 450\,\mu$m and $W = 490\,\mu$m. C_G is the capacitance of the gate to the source/drain, C_{GS} is the capacitance of the gate to the source, and C_{GD} is the capacitance of the gate to the drain. The sum of the minimum capacitance values of C_{GS} and C_{GD} is the minimum value (C_{min}) of C_G. (c) The normalized mobile charge to the area of the channel, which comes from the integration of $(C_G$–$C_{min})/(W \times L)$. (d) The total resistance (R_{total}) as a function of L at different overdrive voltages (V_{GS}–$V_T = -1.3$ V, -1 V, -0.7 V). The contact resistance ($R_{contact}$) can be extracted as 120 kΩ at $L = 0\,\mu$m.

charge (Q_{mobile}) induced in the SWNTs (Eq. (3)) as shown in Figure 3(c). For practical purposes, Eq. (3) is integrated from +4 V. As a consequence, the calculated Q_{mobile} is directly used in the proposed mobility extraction method (Eq. (4)) without the information on Λ_0^{-1} (Ref. 20)

$$Q_{mobile} = \int_{\infty}^{V_{GS}} (C_G - C_{\min}) dV_{GS}/(W \times L), \tag{3}$$

$$\mu = \frac{L}{W} \frac{1}{Q_{mobile} R_{total}}. \tag{4}$$

It was noted earlier that the contact resistance in SWNT TFTs may introduce error into the calculated intrinsic mobility. In Figure 3(d), therefore, the contact resistance was extracted from I_{DS}–V_{GS} measurements (for $V_{DS} = -0.5$ V) of different length SWNT TFTs ($L = 150$, 250, 350, 450 μm) at different V_{GS} values, as described in Ref. 21. For each value of V_{GS}, the V_{DS}/I_{DS} ratio, i.e., the total resistance R_{total}, increases linearly with an increasing L, with the cross point of linear regressions indicating the contact resistance (Eq. (5)). The extracted contact resistance (~120 kΩ) is significantly smaller than the channel resistance for long channel SWNT TFTs ($L = 450$ μm), but it becomes comparable as L decreases

$$R_{total} = \frac{V_{DS}}{I_{DS}} = R_{contact} + R_{channel} = R_{contact} + \frac{L}{\mu C_{OX} W (V_{GS} - V_T)}. \tag{5}$$

Figure 4 shows the extracted mobility based on Eq. (4) and de-embedding $R_{contact}$ for various channel lengths. Each point of mobility in Figure 4 is the average value of 5–7 SWNT TFTs. Although the mobility should be a bulk property, i.e., independent of device channel length and width, it has been commonly observed that the mobility in fact depends on the channel length. There have been different trends in the mobility regarding the channel length, i.e., increased or decreased mobility with channel length, in previous reports.[5,8,14–16] In this work, we observe that the mobility decreases with the channel length because, as the channel length decreases, the effect of $R_{contact}$ becomes more significant, and the mobility correspondingly decreases. This indicates that the mobility in our devices is likely to be limited by $R_{contact}$. Therefore, to extract the intrinsic mobility in a way that is less vulnerable to the $R_{contact}$, we separate the effect of $R_{contact}$ from the R_{total} (Eq. (6))

$$\mu = \frac{L}{W} \frac{1}{Q_{mobile}(R_{total} - R_{contact})}. \tag{6}$$

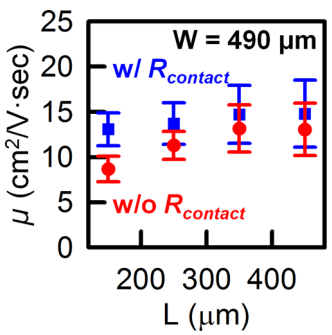

FIG. 4. The red symbol represents the mobility without de-embedding $R_{contact}$ and the blue symbol represents the mobility with de-embedding $R_{contact}$. The values are extracted using the *C-V* and *I-V* characteristics.

We also measure the standard deviation (σ) of the extracted mobility from SWNT TFTs to compare the previous method (cylindrical model) with our method and find that the standard deviation in the previous method ($\sigma = 6.7$–10.9 cm^2/V s) is larger than in our method ($\sigma = 1.4$–2.9 cm^2/V s) because various Λ_0^{-1} values (4–20 tubes/μm) can be taken from the AFM image. In our method, however, we extract an accurate intrinsic mobility regardless of Λ_0^{-1}; therefore, we conclude that the extracted small standard deviation arises only from device variation.

In conclusion, we demonstrate that an accurate extraction of intrinsic mobility in SWNT TFTs can be directly and simply obtained. The previous method of extracting the mobility in SWNT TFTs resulted in several issues with the calculation of SWNT density and the elimination of the contact resistance. By using *C-V* and *I-V* measurements, we resolve the inadequacy of the previous method. Therefore, we expect that the method proposed in this paper will serve as a guideline for future research in this field.

This work was supported by the National Research Foundation of Korea through the Ministry of Education, Science and Technology, Korean Government (Grant No. 2013057870), in part by the National Research Foundation of Korea (Grant Nos. 2013R1A1A3011492 and 2013K14A3055679), in part by BK21+ with the Educational Research Team for Creative Engineers on Material-Device-Circuit Co-Design (Grant No. 22A20130000042), in part by the Center for Integrated Smart Sensors funded by the Ministry of Science, ICT & Future Planning as a Global Frontier Project (Grant No. CISS-2011-0031848), and in part by the National Research Foundation of Korea funded by the Ministry of Science, ICT & Future Planning, Korean Government (Grant No. 2012-0009594).

[1]E. S. Snow, J. P. Novak, P. M. Campbell, and D. Park, Appl. Phys. Lett. **82**, 2145 (2003).
[2]E. S. Snow, P. M. Campbell, and M. G. Ancona, Appl. Phys. Lett. **86**, 033105 (2005).
[3]Q. Cao, H. S. Kim, N. Pimparkar, J. P. Kulkarni, C. Wang, M. Shim, K. Roy, M. A. Alam, and J. A. Rogers, Nature **454**, 495 (2008).
[4]Q. Cao and J. A. Rogers, Adv. Mater. **21**, 29 (2009).
[5]C. Wang, J. Zhang, K. Ryu, A. Badmaev, L. G. De Arco, and C. Zhou, Nano Lett. **9**, 4285 (2009).
[6]M. Kaempgen, C. K. Chan, J. Ma, Y. Cui, and G. Gruner, Nano Lett. **9**, 1872 (2009).
[7]J. Zhang, C. Wang, Y. Fu, Y. Che, and C. Zhou, ACS Nano **5**, 3284 (2011).
[8]C. Wang, J. Zhang, and C. Zhou, ACS Nano **4**, 7123 (2010).
[9]Y. Zhou, A. Gaur, S. H. Hur, C. Kocabas, M. A. Meitl, M. Shim, and J. A. Rogers, Nano Lett. **4**, 2031 (2004).
[10]A. Behnam, V. K. Sangwan, X. Zhong, F. Lian, D. Estrada, D. Jariwala, A. J. Hoag, L. J. Lauhon, T. J. Marks, M. C. Hersam, and E. Pop, ACS Nano **7**, 482 (2012).
[11]M. Y. Timmermans, D. Estrada, A. G. Nasibulin, J. D. Wood, A. Behnam, D. M. Sun, Y. Ohno, J. W. Lyding, A. Hassanien, E. Pop, and E. I. Kauppinen, Nano Res. **5**, 307 (2012).
[12]X. Z. Bo, N. G. Tassi, C. Y. Lee, M. S. Strano, C. Nuckolls, and G. B. Blanchet, Appl. Phys. Lett. **87**, 203510 (2005).

[13]C. Wang, J. C. Chien, K. Takei, T. Takahashi, J. Nah, A. M. Niknejad, and A. Javey, Nano Lett. **12**, 1527 (2012).
[14]Q. Cao, M. G. Xia, M. Shim, and J. A. Rogers, Adv. Funct. Mater. **16**, 2355 (2006).
[15]N. Rouhi, D. Jain, K. Zand, and P. J. Burke, Adv. Mater. **23**, 94 (2011).
[16]N. Rouhi, D. Jain, and P. J. Burke, ACS Nano **5**, 8471 (2011).
[17]S. J. Choi, C. Wang, C. C. Lo, P. Bennett, A. Javey, and J. Bokor, Appl. Phys. Lett. **101**, 112104 (2012).
[18]T. Takahashi, K. Takei, A. G. Gillies, R. S. Fearing, and A. Javey, Nano Lett. **11**, 5408 (2011).
[19]Q. Cao, M. Xia, C. Kocabas, M. Shim, and J. A. Rogers, Appl. Phys. Lett. **90**, 023516 (2007).
[20]K. Ryu, I. Kymissis, V. Bulovic, and C. G. Sodini, IEEE Electron Device Lett. **26**, 716 (2005).
[21]Y. Taur and T. H. Ning, *Fundamentals of Modern VLSI Devices* (Cambridge University Press, Cambridge, 1998), p. 244.